Atlas of Formability

Waspaloy

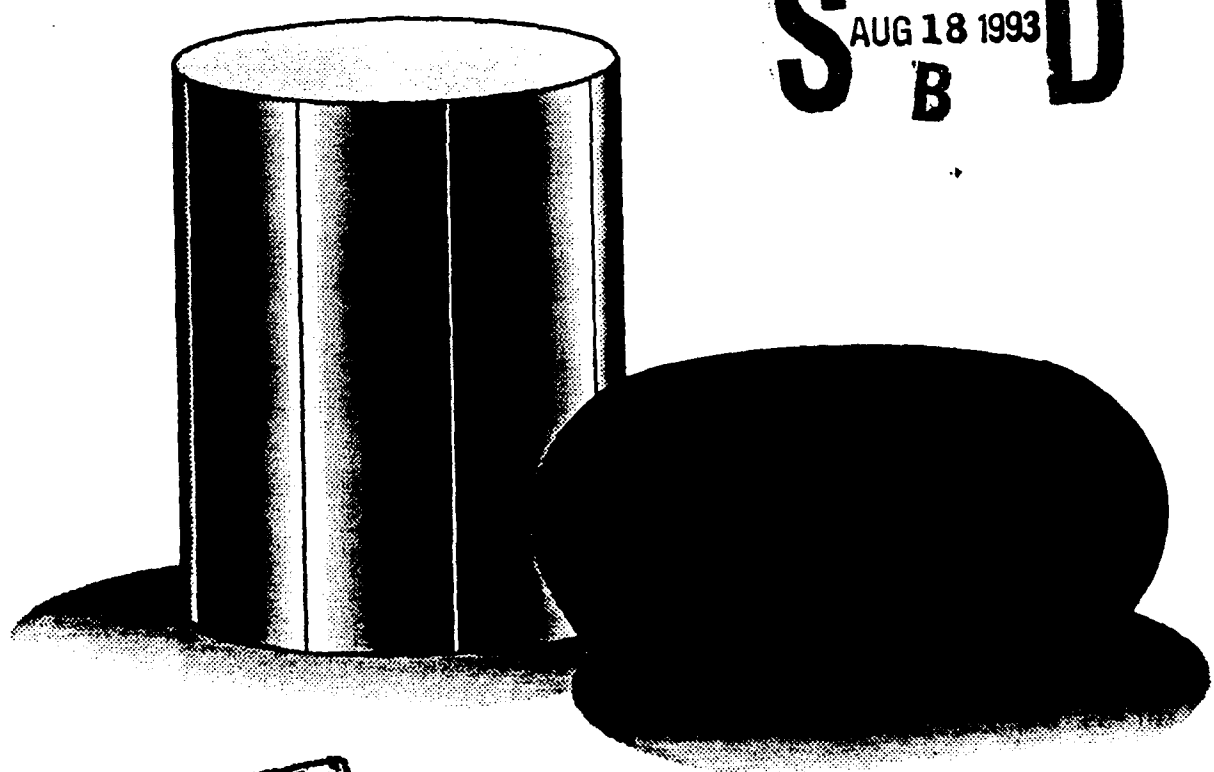

NCEMT

DISCLAIMER NOTICE

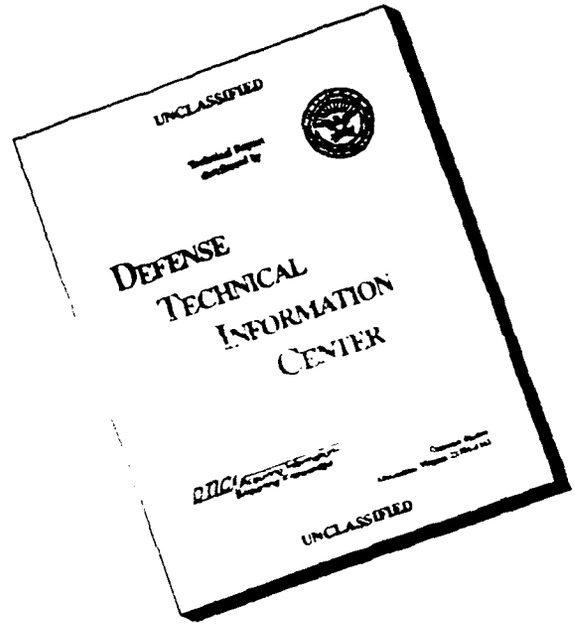

THIS DOCUMENT IS BEST QUALITY AVAILABLE. THE COPY FURNISHED TO DTIC CONTAINED A SIGNIFICANT NUMBER OF PAGES WHICH DO NOT REPRODUCE LEGIBLY.

ATLAS OF FORMABILITY

WASPALOY

by

Prabir K. Chaudhury and Dan Zhao

National Center for Excellence in Metalworking Technology
1450 Scalp Avenue
Johnstown, PA 15904

for

Naval Industrial Resource Support Activity
Building 75-2, Naval Base
Philadelphia, PA 19112-5078

July 31, 1992

REPORT DOCUMENTATION PAGE

Form Approved
OMB No. 0704-0188

1. AGENCY USE ONLY (Leave blank)	2. REPORT DATE	3. REPORT TYPE AND DATES COVERED
	July 31, 1992	Final, April 30, 1992-July 31, 1992

4. TITLE AND SUBTITLE

Atlas of Formability
Waspaloy

5. FUNDING NUMBERS

C-N00140-88-C-RC21

6. AUTHOR(S)

Prabir K. Chaudhury
Dan Zhao

7. PERFORMING ORGANIZATION NAME(S) AND ADDRESS(ES)

National Center for Excellence in Metalworking
Technology (NCEMT)
1450 Scalp Avenue
Johnstown, PA 15904

8. PERFORMING ORGANIZATION REPORT NUMBER

9. SPONSORING/MONITORING AGENCY NAME(S) AND ADDRESS(ES)

Naval Industrial Resources Support Activity
Building 75-2, Naval Base
Philadelphia, PA 19112-5078

10. SPONSORING/MONITORING AGENCY REPORT NUMBER

11. SUPPLEMENTARY NOTES

12a. DISTRIBUTION/AVAILABILITY STATEMENT

12b. DISTRIBUTION CODE

13. ABSTRACT *(Maximum 200 words)*

In this investigation, flow behavior of Waspaloy alloy was studied by conducting compression tests overr awide range of temperautres and strain rates. Constitutive relations were determined from the flow behavior, and a dynamic material modeling was conducted on this alloy. Thus, the optimum processing condition in terms of temperature and strain rate was identified. Microstructural changes during high temperature deformation were also characterized.

14. SUBJECT TERMS

Waspaloy, Deformation Processing, High Temperature Deformation, Processing Map, Metalworking

15. NUMBER OF PAGES

31

16. PRICE CODE

17. SECURITY CLASSIFICATION OF REPORT	18. SECURITY CLASSIFICATION OF THIS PAGE	19. SECURITY CLASSIFICATION OF ABSTRACT	20. LIMITATION OF ABSTRACT
Unclassified	Unclassifed	Unclassified	

TABLE OF CONTENTS

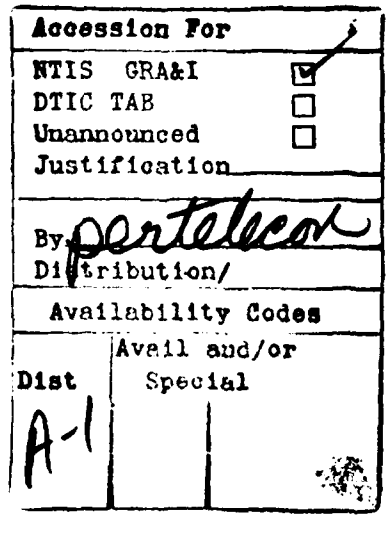

LIST OF TABLE

Waspaloy

Introduction

High performance requirements in the application of superalloys, such as aircraft gas turbines, has increased the need to understand both the mechanical and microstructural behavior of superalloys in metalworking processes. Flow behavior of Waspaloy through compression testing at various temperatures and strain rates was performed to determine the constitutive relations. From the constitutive relations a dynamic material modeling on Waspaloy was carried out to optimize processing conditions such as temperature and strain rate. In addition, microstructural changes were characterized to show the effect of temperature and strain rate on the resulting deformed microstructure. In some forming practices of superalloys, high strain rates are often encountered during the processing, such as hammer forging. Thus the present study extends the testing strain rate up to 25 s^{-1}.

Experimental Procedure

Commercially available Waspaloy wrought bars in the heat treated and aged condition was tested. Typical microstructure of the as-received materials showing equiaxed grains is shown in Figure 1. The initial grain size was 25 μm (7.5ASTM).

Cylindrical compression test specimens with a diameter of 12.7 mm and a height of 15.9 mm were machined, and compression tests were conducted isothermally on an MTS testing machine. Boron nitride lubricant was applied to reduce friction. The temperatures selected include those which are both above and under γ' (1040 C) solvus. The test matrix was as follows:

Temperature, C (F): 982 (1800), 1010 (1850), 1038 (1900), 1079 (1975) and 1149 (2100);
Strain rate, s^{-1}: 0.01, 0.14, 1.84 and 25.

Load and stroke data from the tests were acquired by a microcomputer and later converted to true stress-true strain curves. Immediately after the compression test, the specimens were quenched in order to retain the deformed microstructure. Longitudinal and transverse sections of the quenched specimens were examined using optical microscope. The photomicrographs presented were taken from the center of the longitudinal section of the specimens.

Results

Table 1 is a list of the figures, test conditions and the deformed microstructures observed. All the true stress-true strain flow curves with the corresponding microstructure are shown in Figure 2 to Figure 21. True stress versus strain rate was plotted in log-log scale in Figure 22 at a true strain of 0.5. The slope of the plot gave the strain rate sensitivity m, which is not constant over the range of strain rate tested. Log stress vs. 1/T at the same true strain is shown in Figure 23. A processing map at this strain was developed for Waspaloy and it is shown in Figure 24. The optimum processing conditions from the map can be obtained by selecting the temperature and strain rate combination which provides the maximum efficiency in the stable region. This condition is approximately 1080 C (1975 F) at the lowest strain rate tested, 0.01 s^{-1}.

Table 1. List of figures, testing conditions and microstructural observations.

Figure No	Temperature C (F)	Strain Rate S^{-1}	Microstructure Optical Microscopy	Page No
1			As-received: Equiaxed grains with an average size of 25 μm. A small proportion of larger grains (40-50μm) present.	3
2	982(1800)	0.01	Deformed grains with extensive grain boundary precipitation. Presence of some very large isolated deformed grains.	4
3	982(1800)	0.14	Same as above, but with a less proportion of fine precipitates at the grain boundaries.	5
4	982(1800)	1.84	Same as above, but the proportion of fine precipitates kept decreasing.	6
5	982(1800)	25.00	Same as above (testing performed in an inert gas atmosphere).	7
6	1010(1850)	0.01	Deformed grains with some grain boundary precipitation. "Serrated" grain boundaries (initiation for dynamic recrystallization). Some necklacing present.	8
7	1010(1850)	0.14	Same as above.	9
8	1010(1850)	1.84	Same as above, but necklacing is more evident.	10
9	1010(1850)	25.00	Same as above and necklacing is well defined.	11
10	1038(1900)	0.01	Small and equiaxed dynamically recrystallized grains, presence of twins. There is still the presence of large grains (35-45 μm).	12
11	1038(1900)	0.14	Same as above.	13
12	1038(1900)	1.84	Same as above, but the proportion of twins increased.	14
13	1038(1900)	25.00	Equiaxed duplex grain size; small grains (~20μm) and relatively large grains (~40μm). Note that 1038 C is just bellow the γ'solvus.	15
14	1079(1975)	0.01	Large equiaxed grains (~30μm).	16
15	1079(1975)	0.14	Equiaxed and heavily twinned grains with a size smaller than above.	17
16	1079(1975)	1.84	Same as above, but smaller grain size (~25μm).	18
17	1079(1975)	25.00	Equiaxed grains, but smaller than above.	19
18	1149(2100)	0.01	Very large equiaxed grains (60-65μm), presence of twins.	20
19	1149(2100)	0.14	Same as above, but smaller grain size (~55μm).	21
20	1149(2100)	1.84	Same as above.	22
21	1149(2100)	25	Smaller grains than above.	23

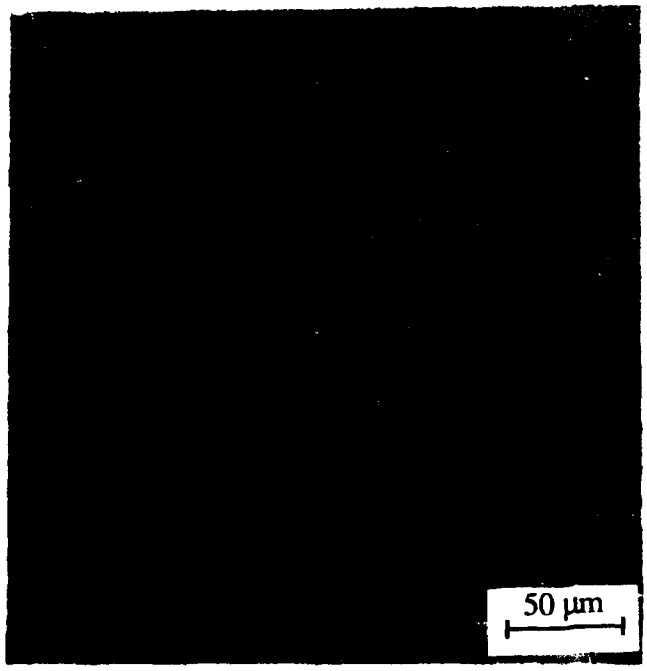

Figure 1. As-received microstructure of Waspaloy.

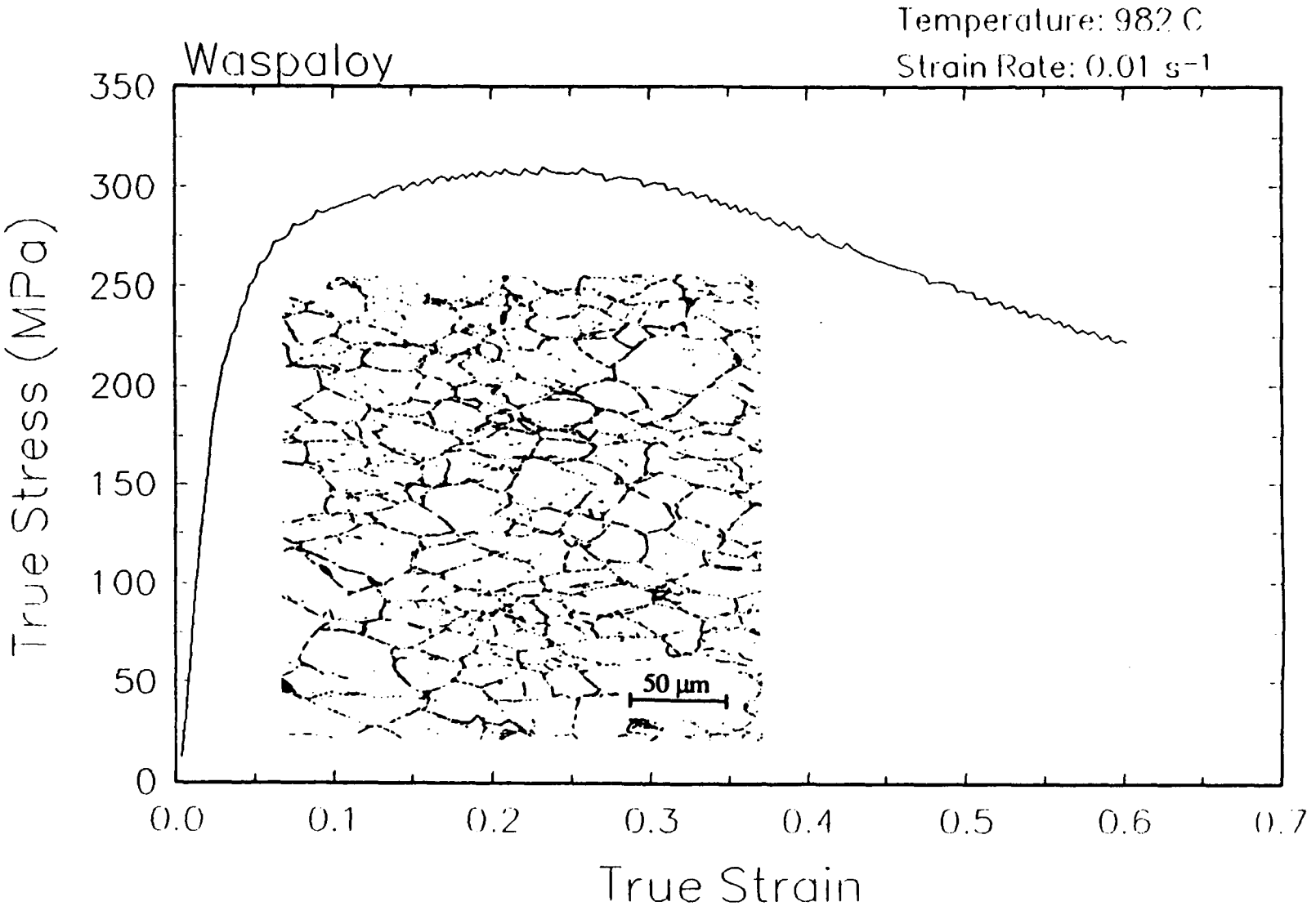

Figure 2. True stress-true strain curve and an optical micrograph from the center of the compressed sample cut through the compression axis, 982 C and 0.01 s^{-1}.

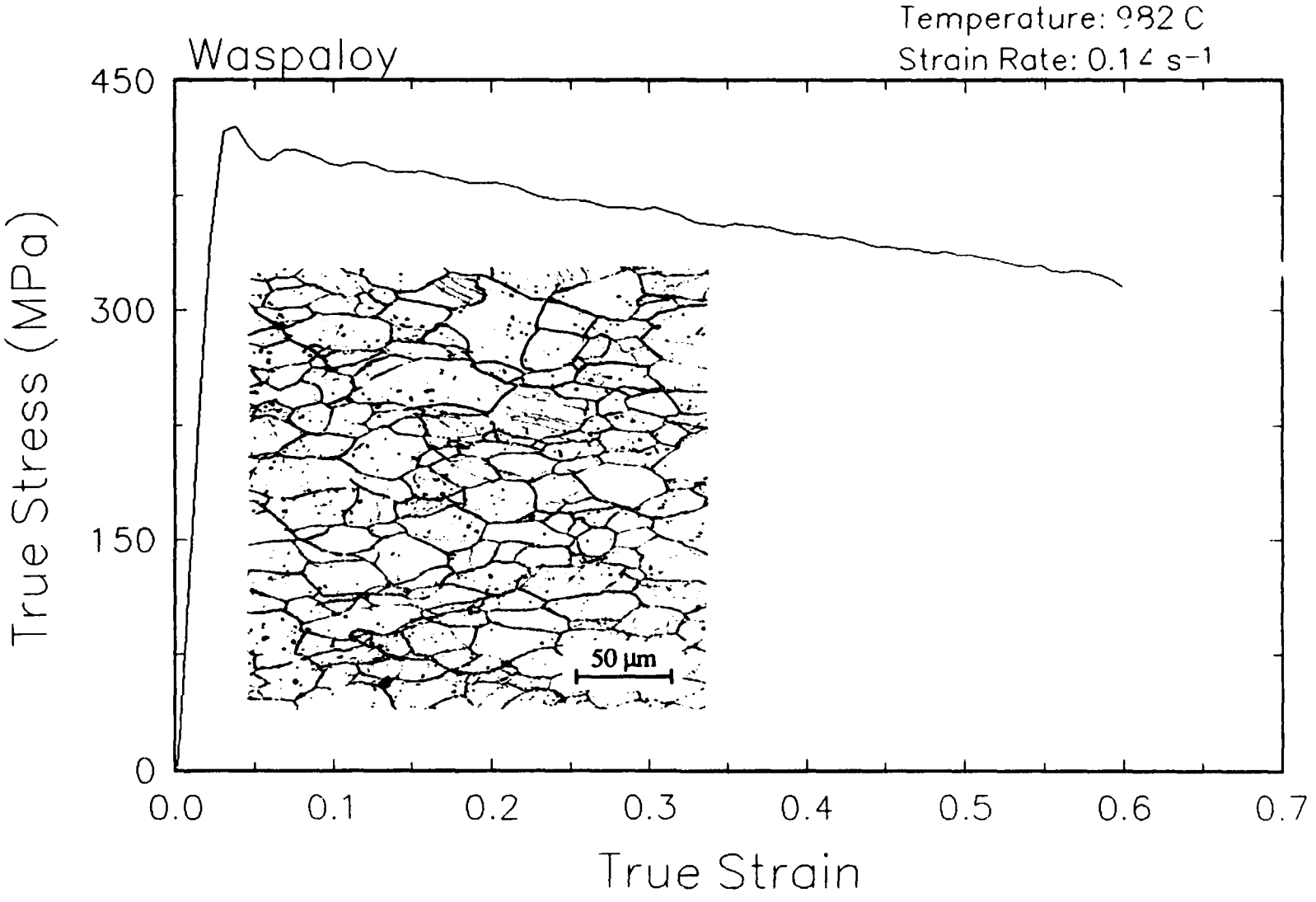

Figure 3. True stress-true strain curve and an optical micrograph from the center of the compressed sample cut through the compression axis, 982 C and 0.14 s^{-1}.

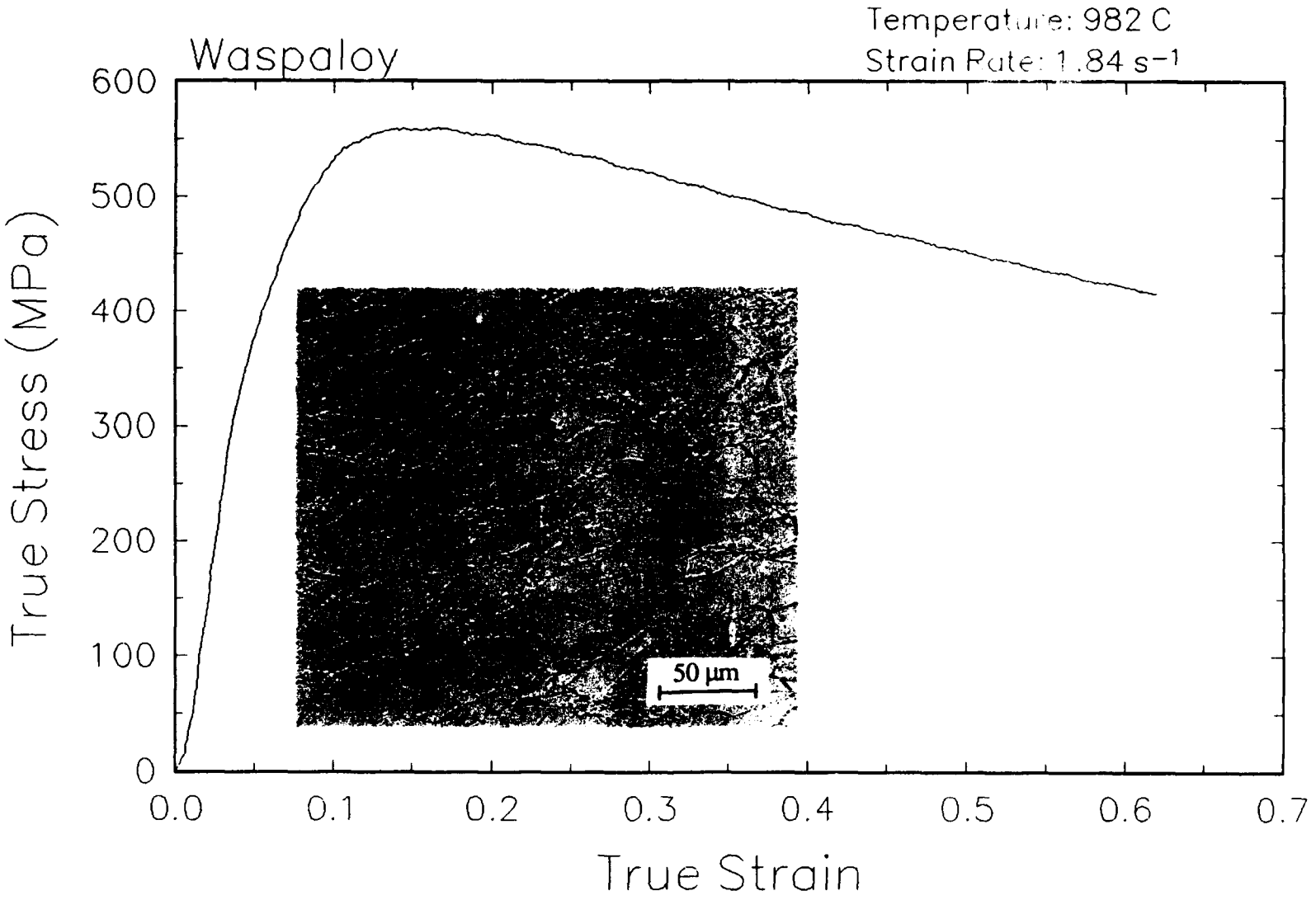

Figure 4. True stress-true strain curve and an optical micrograph from the center of the compressed sample cut through the compression axis, 982 C and 1.84 s^{-1}.

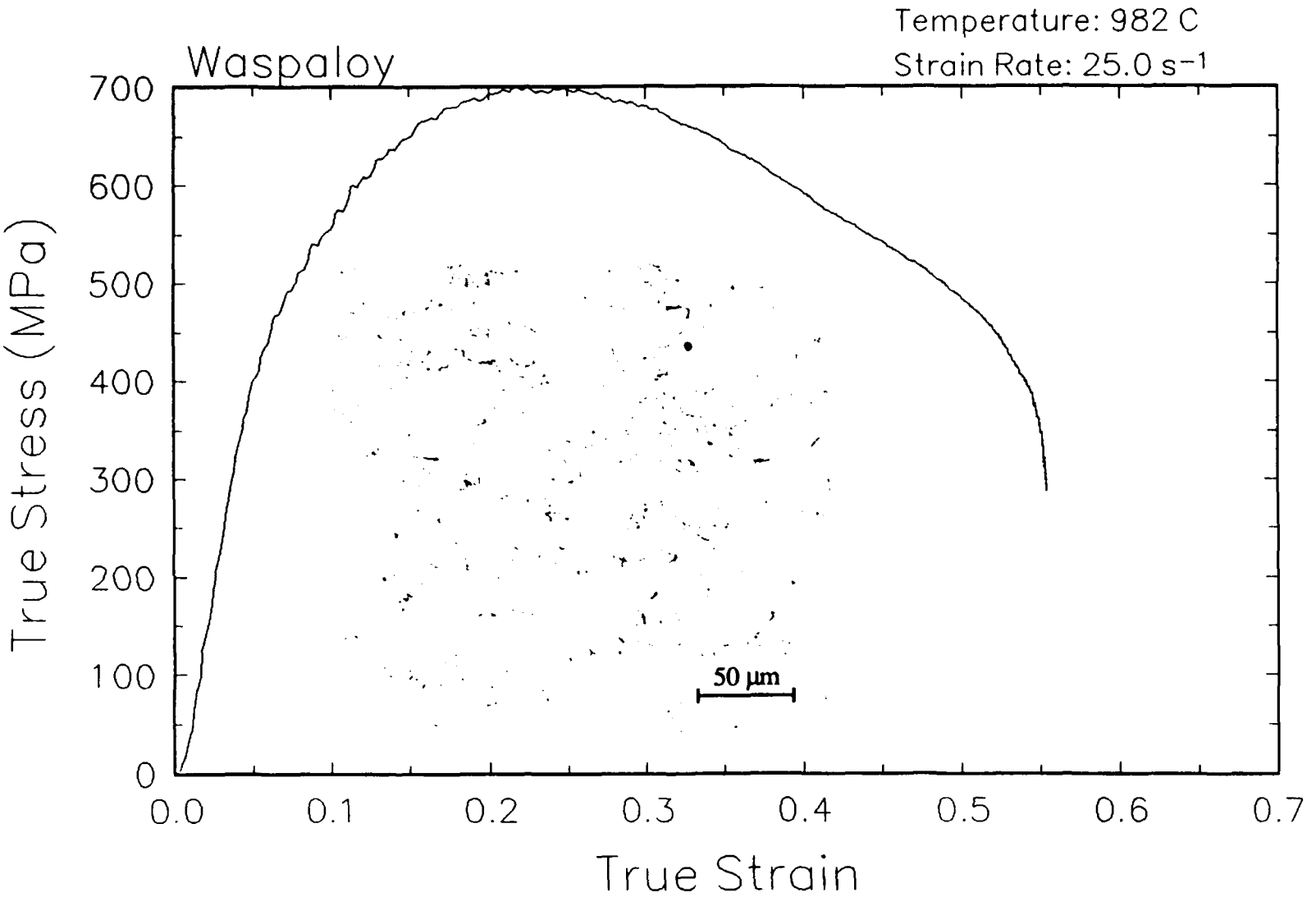

Figure 5. True stress-true strain curve and an optical micrograph from the center of the compressed sample cut through the compression axis, 982 C and 25 s^{-1}.

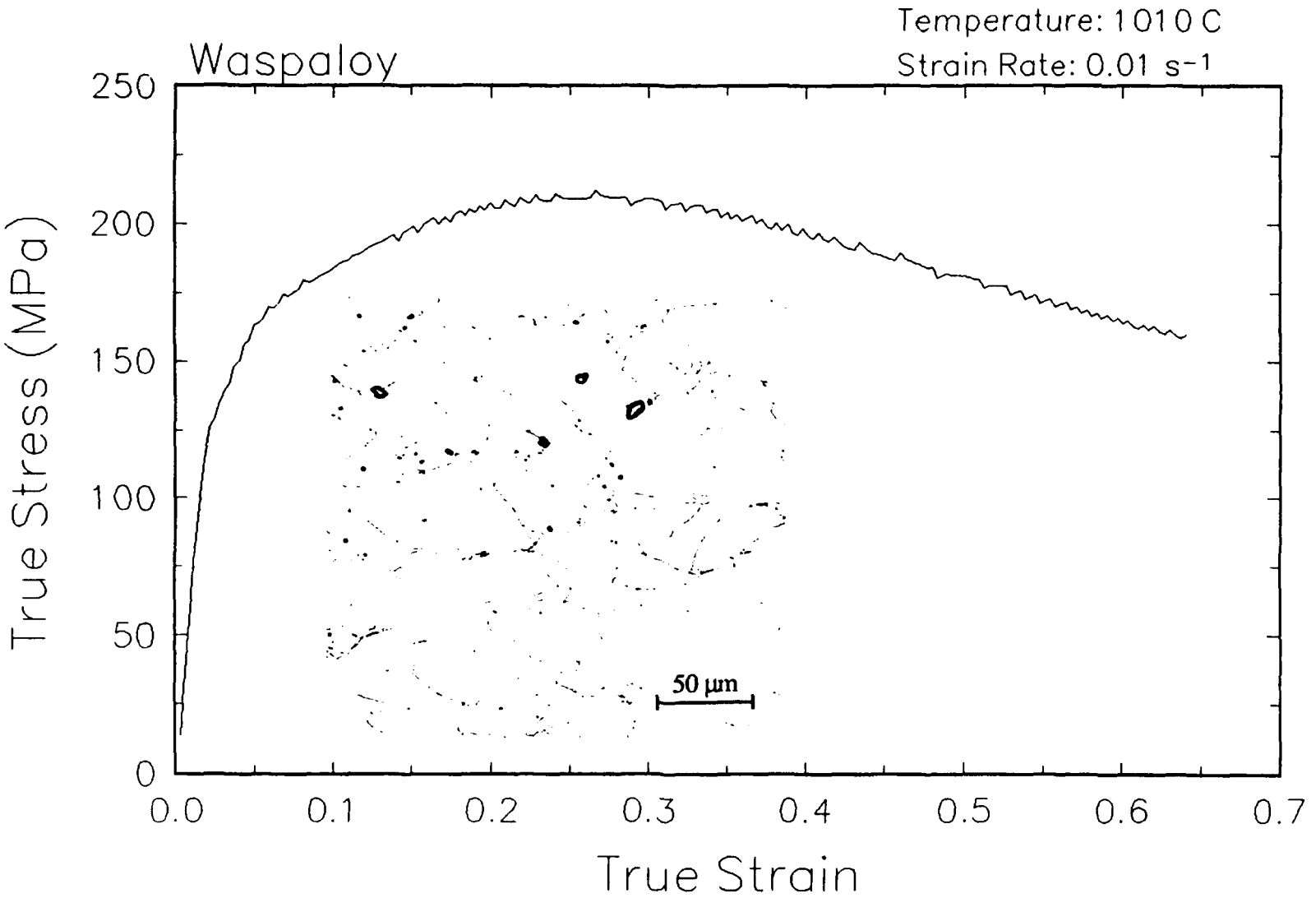

Figure 6. True stress-true strain curve and an optical micrograph from the center of the compressed sample cut through the compression axis, 1010 C and 0.01 s^{-1}.

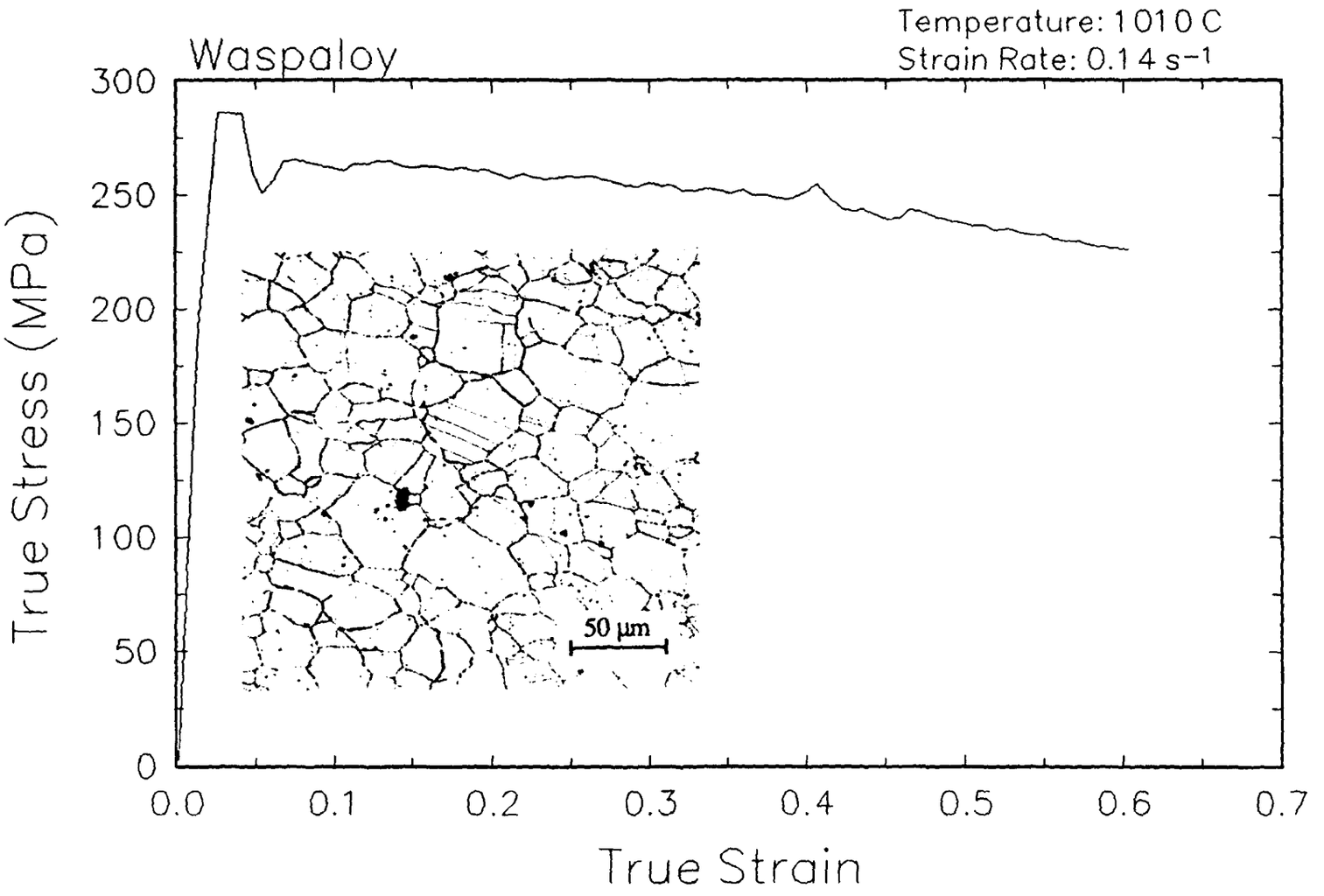

Figure 7. True stress-true strain curve and an optical micrograph from the center of the compressed sample cut through the compression axis, 1010 C and 0.14 s^{-1}.

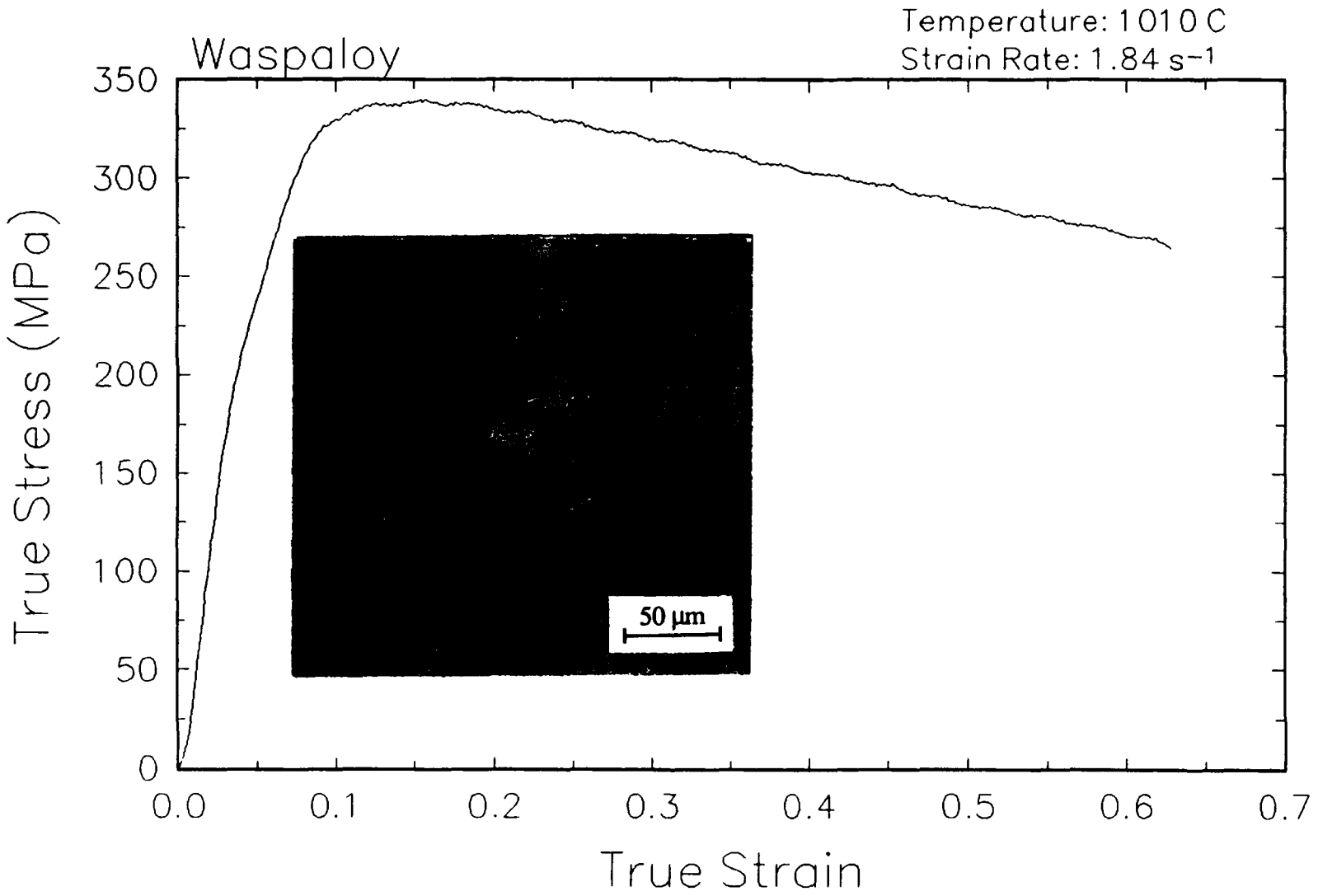

Figure 8. True stress-true strain curve and an optical micrograph from the center of the compressed sample cut through the compression axis, 1010 C and 1.84 s^{-1}.

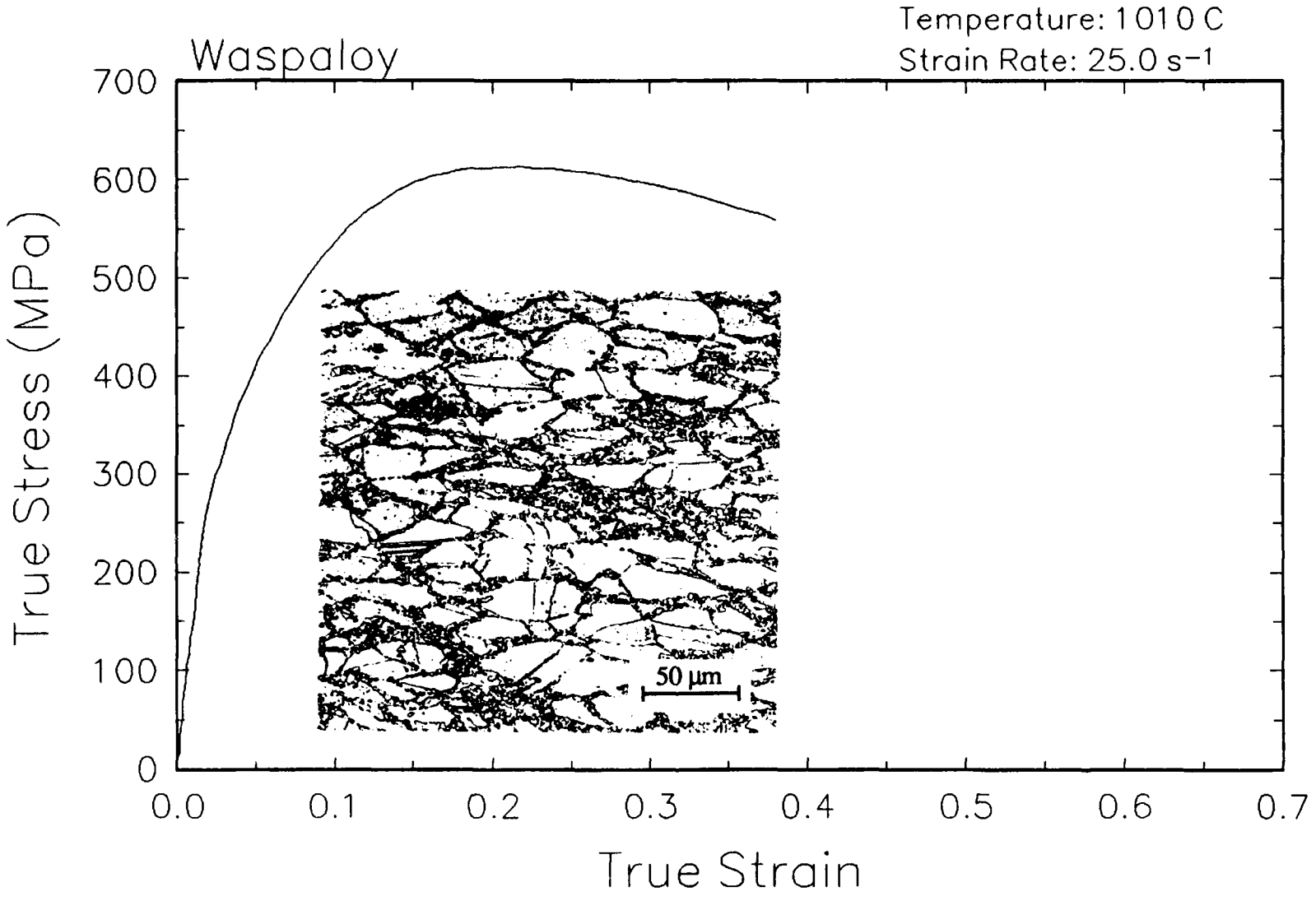

Figure 9. True stress-true strain curve and an optical micrograph from the center of the compressed sample cut through the compression axis, 1010 C and 25 s^{-1}.

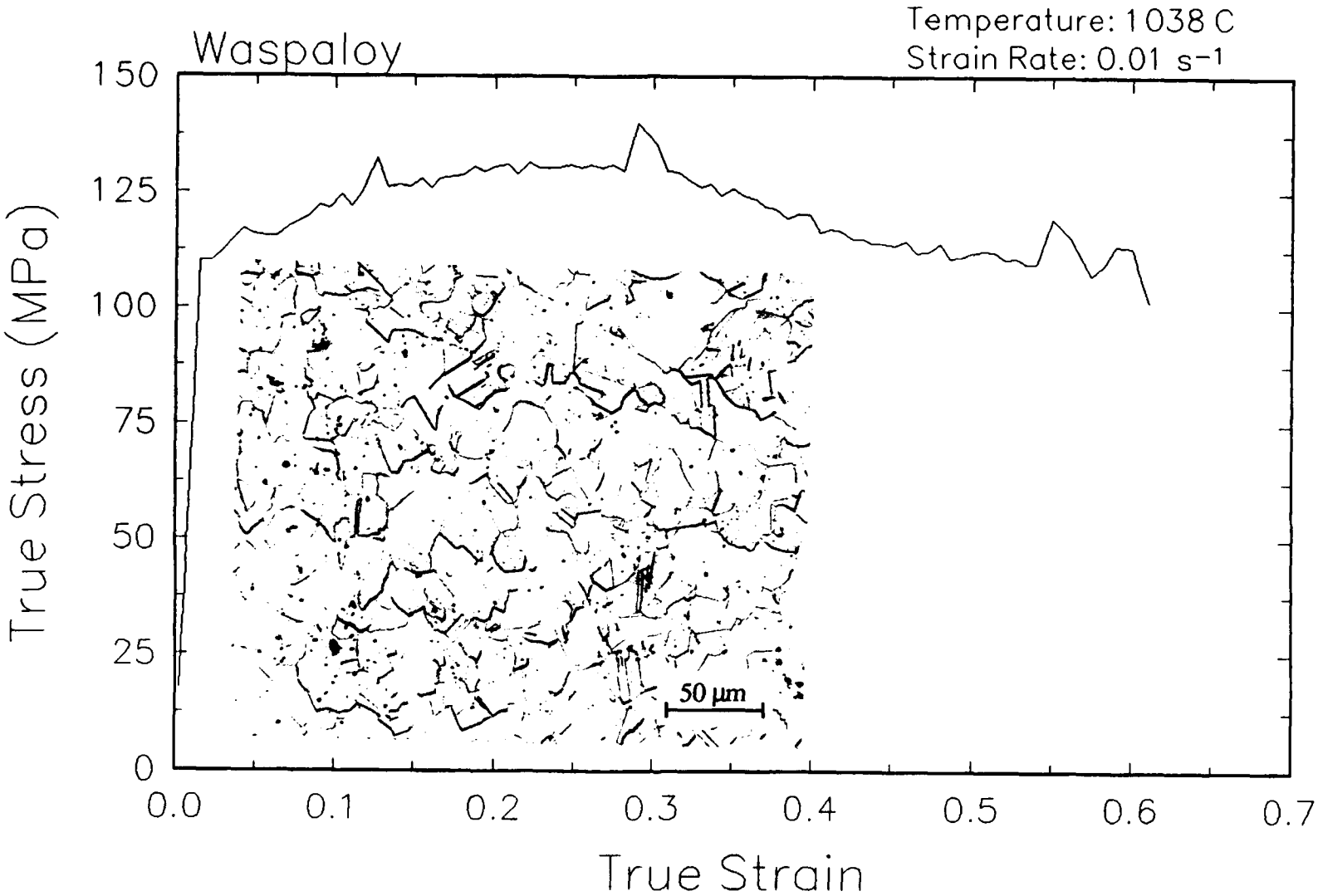

Figure 10. True stress-true strain curve and an optical micrograph from the center of the compressed sample cut through the compression axis, 1038 C and 0.01 s^{-1}.

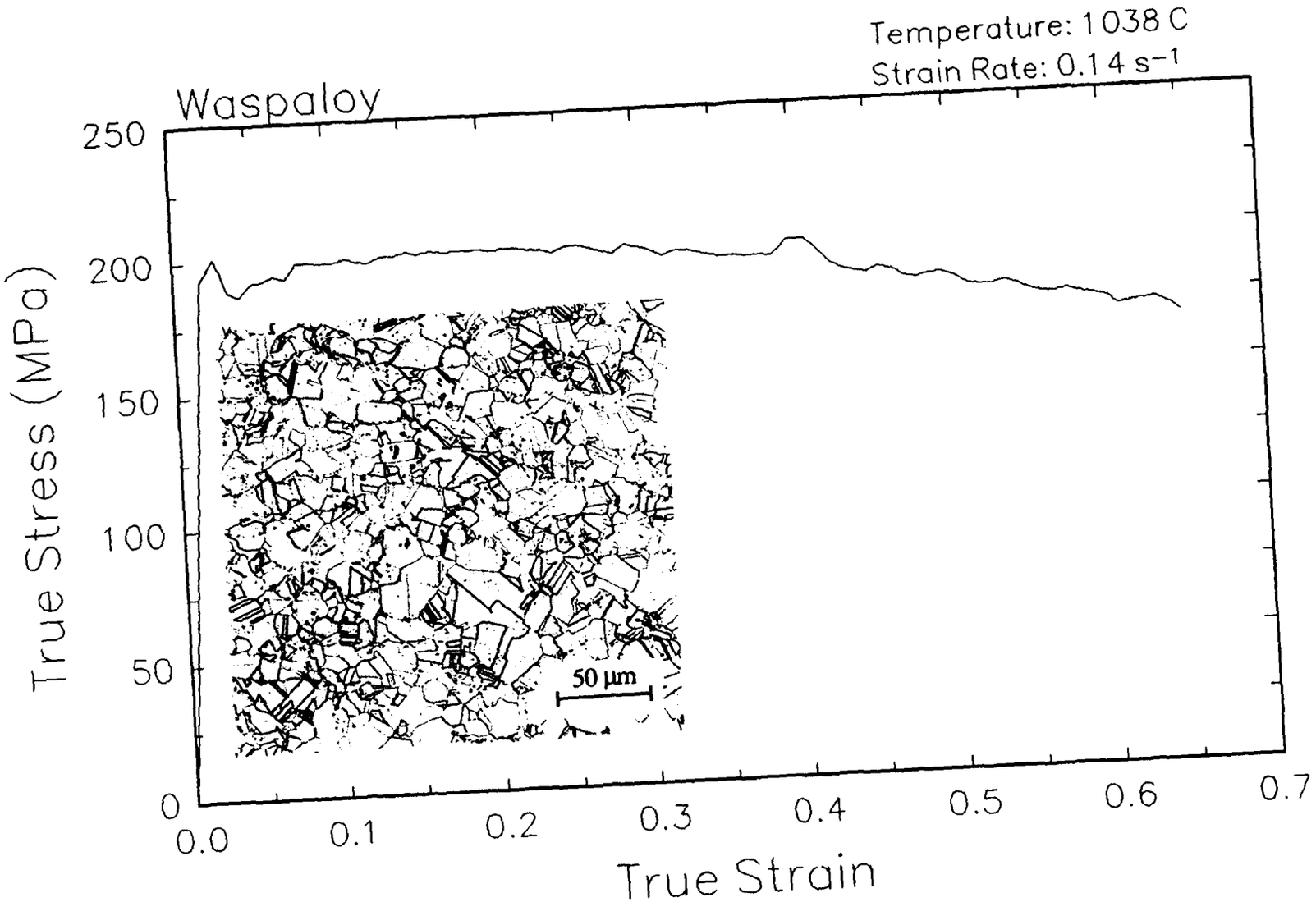

Figure 11. True stress-true strain curve and an optical micrograph from the center of the compressed sample cut through the compression axis, 1038 C and 0.14 s^{-1}.

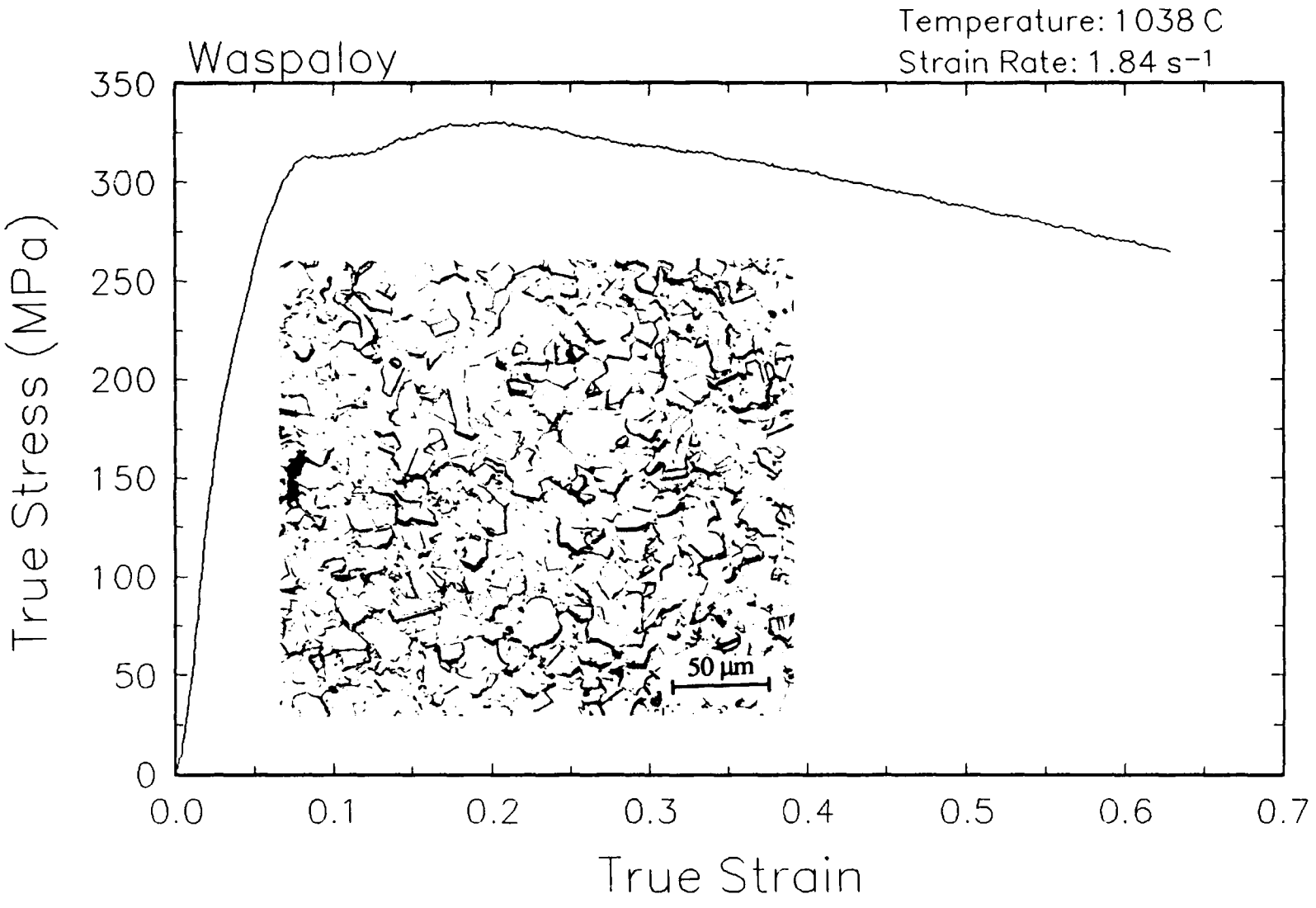

Figure 12. True stress-true strain curve and an optical micrograph from the center of the compressed sample cut through the compression axis, 1038 C and 1.84 s^{-1}.

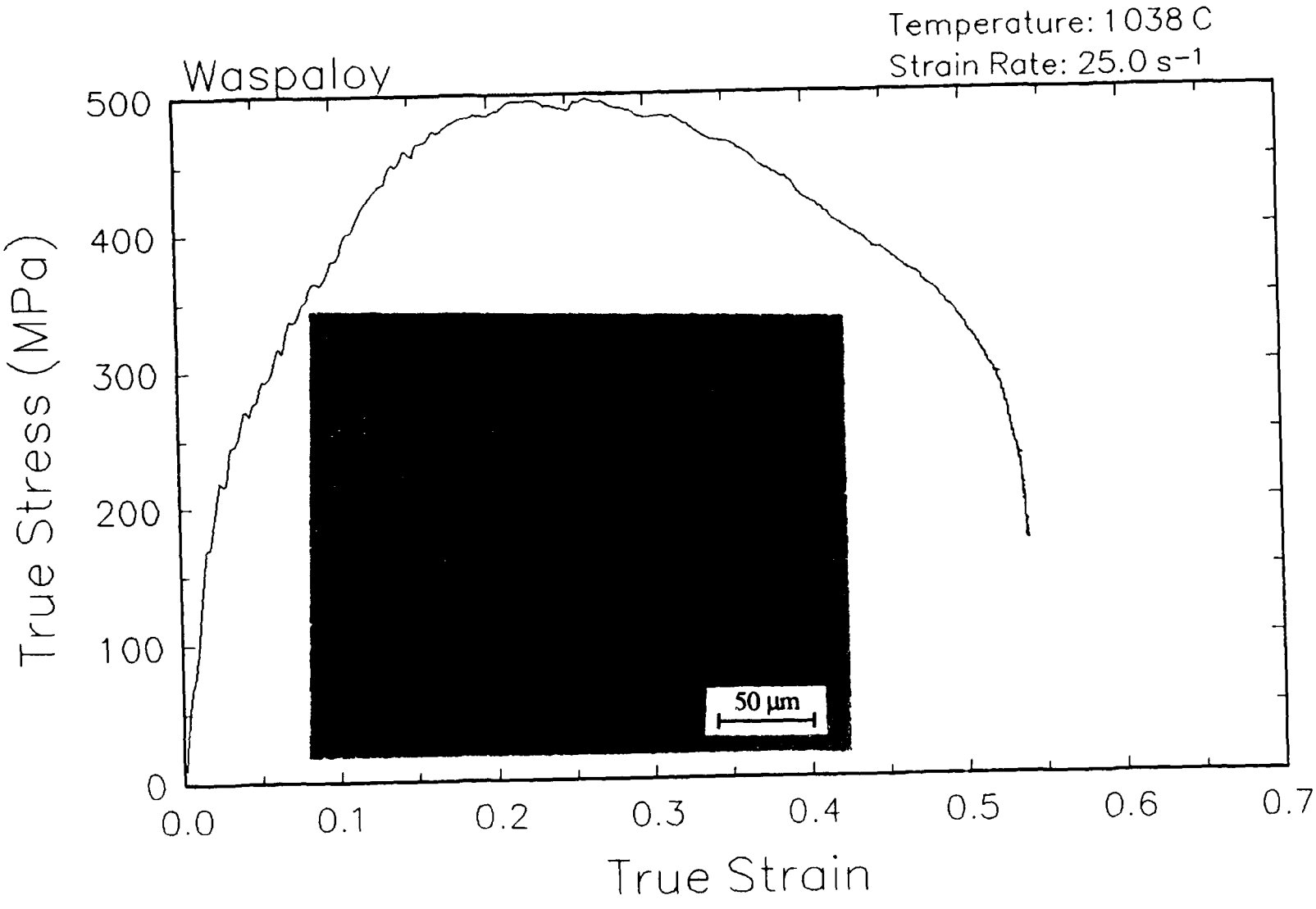

Figure 13. True stress-true strain curve and an optical micrograph from the center of the compressed sample cut through the compression axis, 1038 C and 25 s^{-1}.

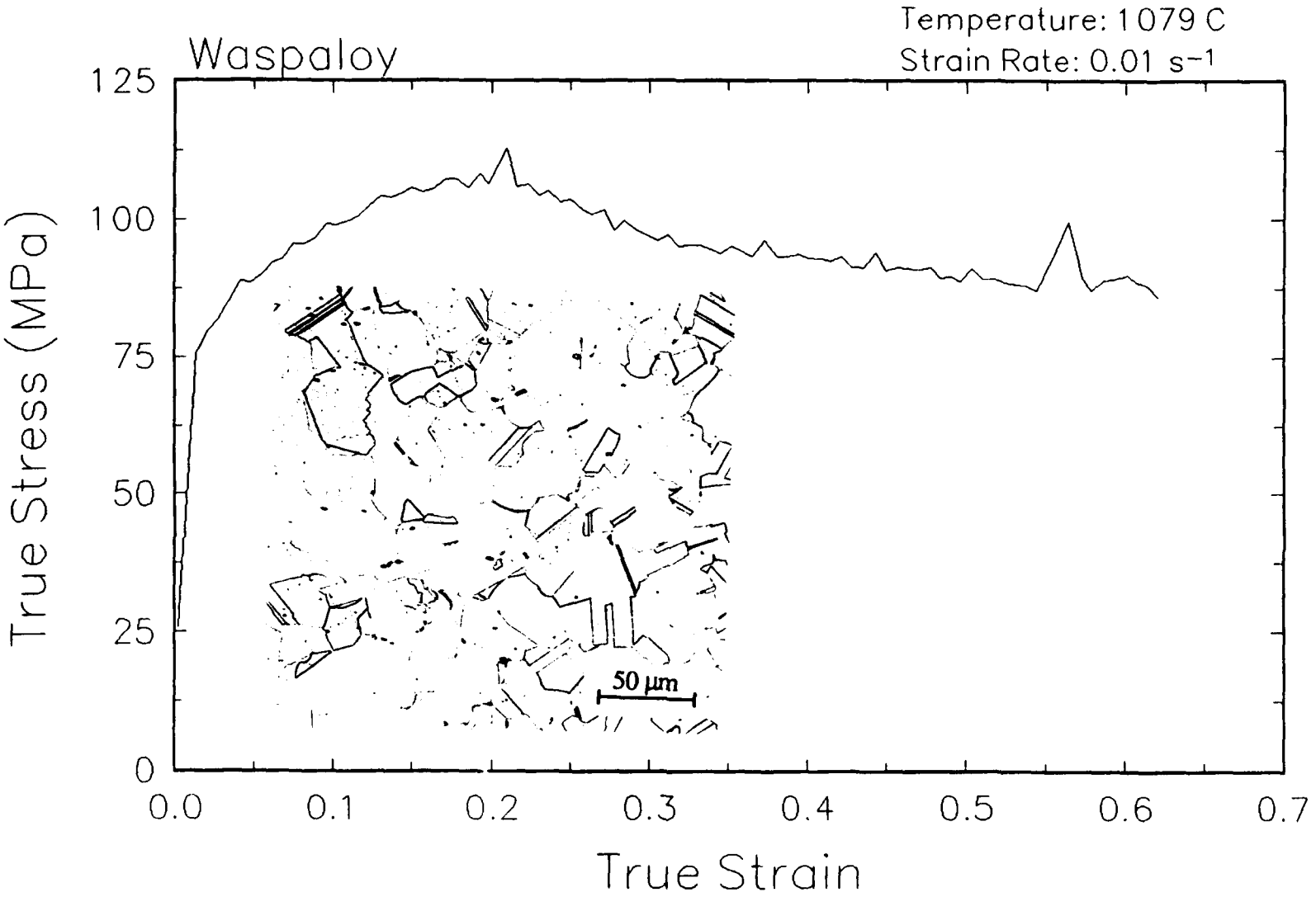

Figure 14. True stress-true strain curve and an optical micrograph from the center of the compressed sample cut through the compression axis, 1079 C and 0.01 s^{-1}.

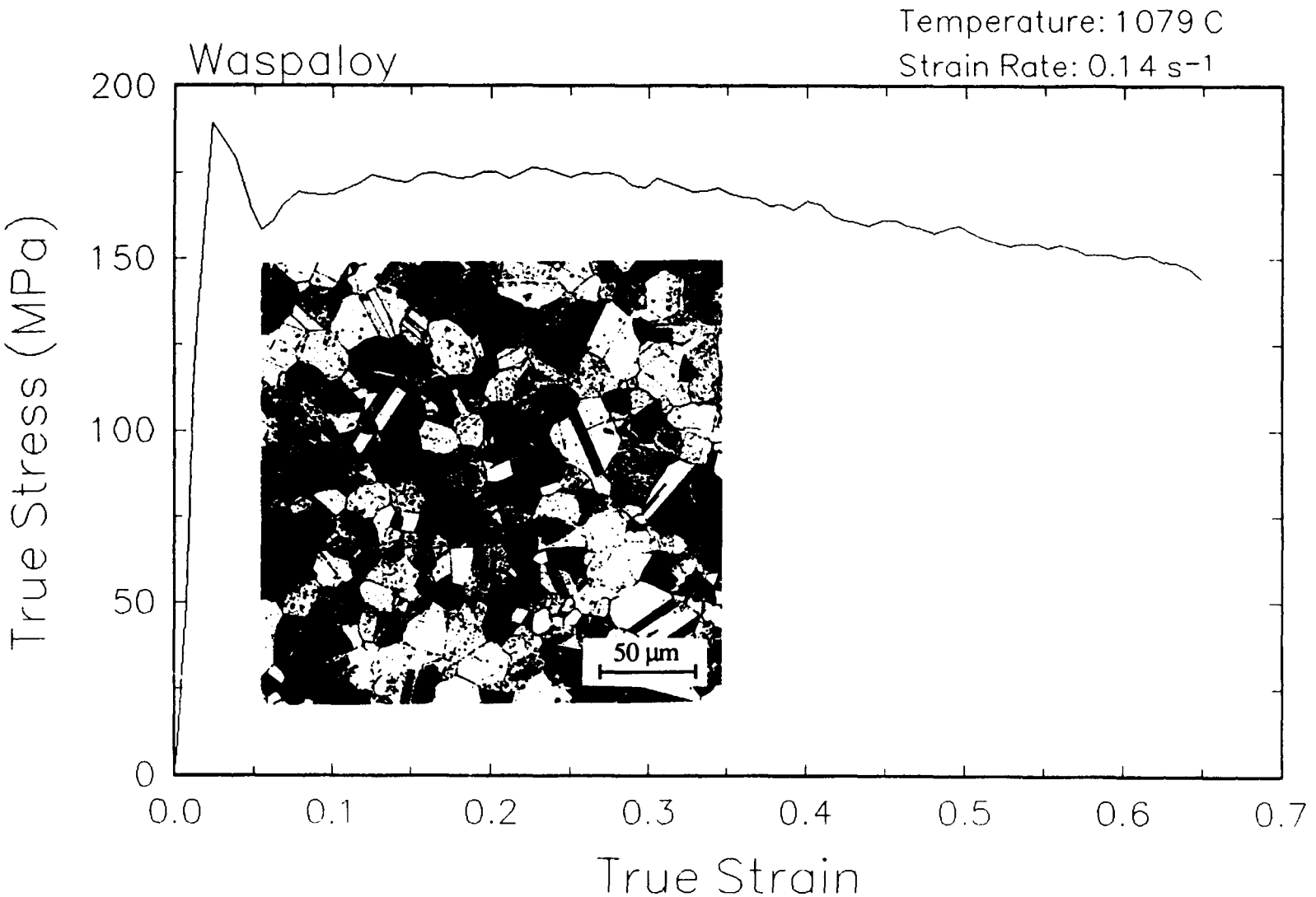

Figure 15. True stress-true strain curve and an optical micrograph from the center of the compressed sample cut through the compression axis, 1079 C and 0.14 s^{-1}.

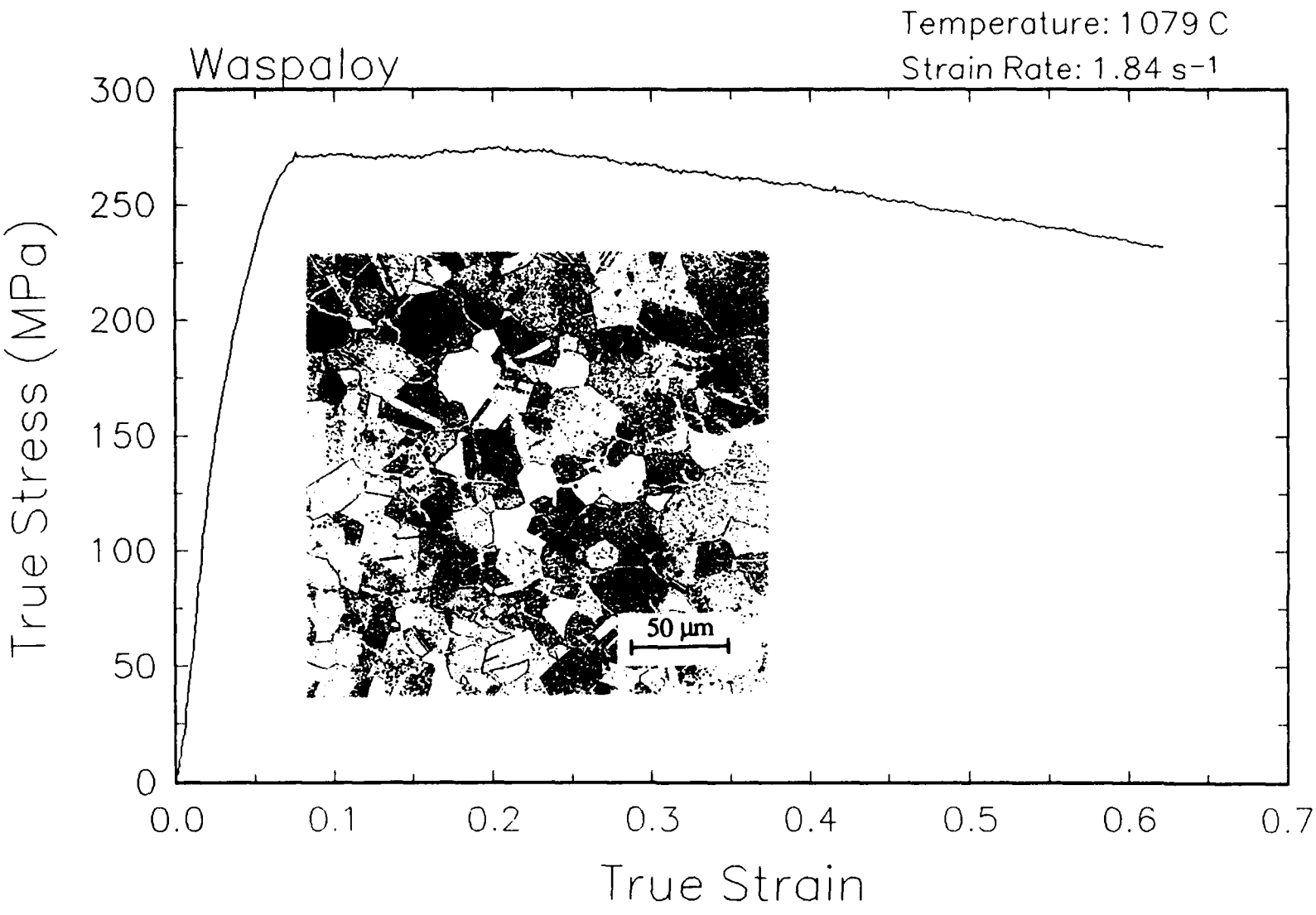

Figure 16. True stress-true strain curve and an optical micrograph from the center of the compressed sample cut through the compression axis, 1079 C and 1.84 s^{-1}.

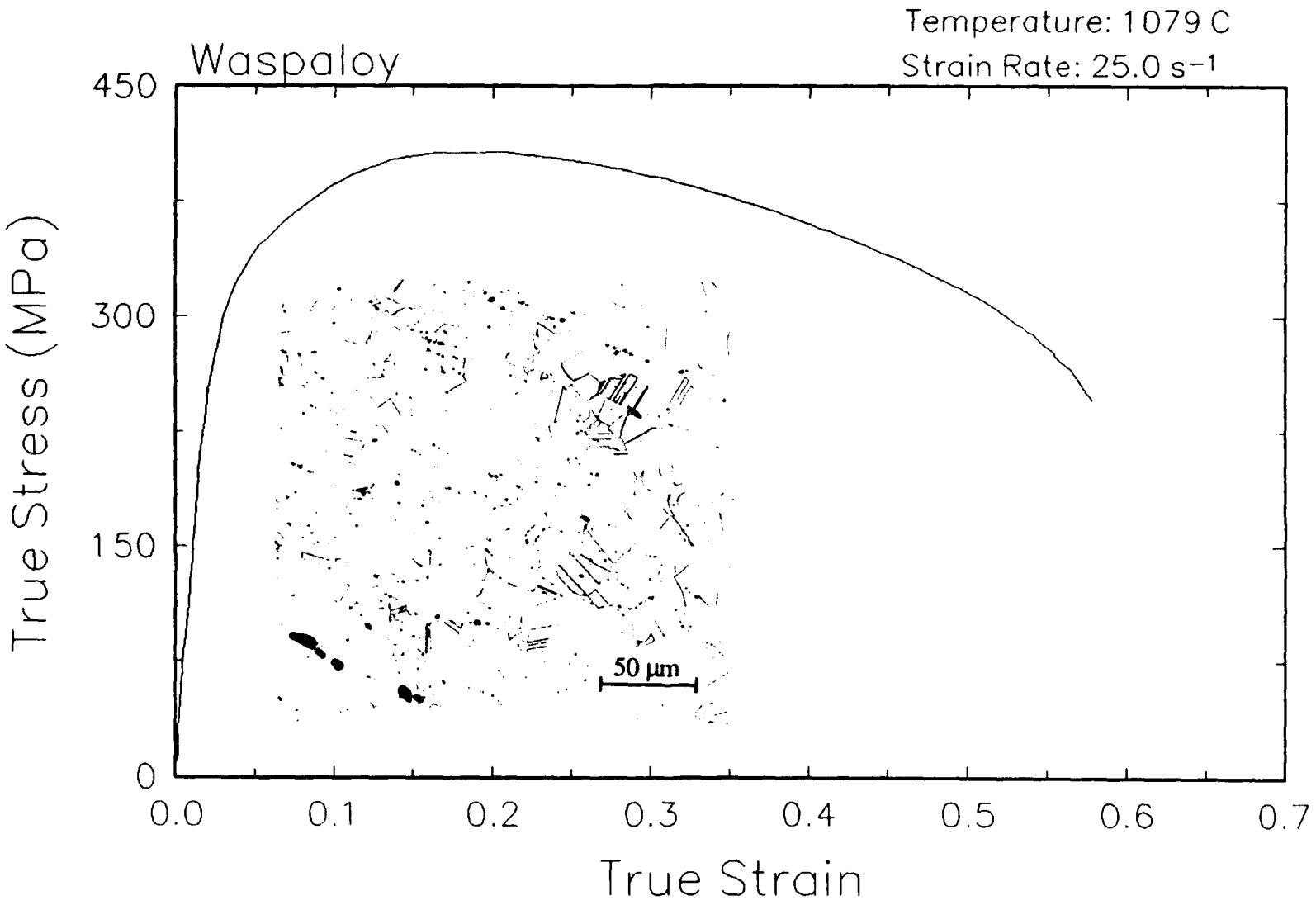

Figure 17. True stress-true strain curve and an optical micrograph from the center of the compressed sample cut through the compression axis, 1079 C and 25 s^{-1}.

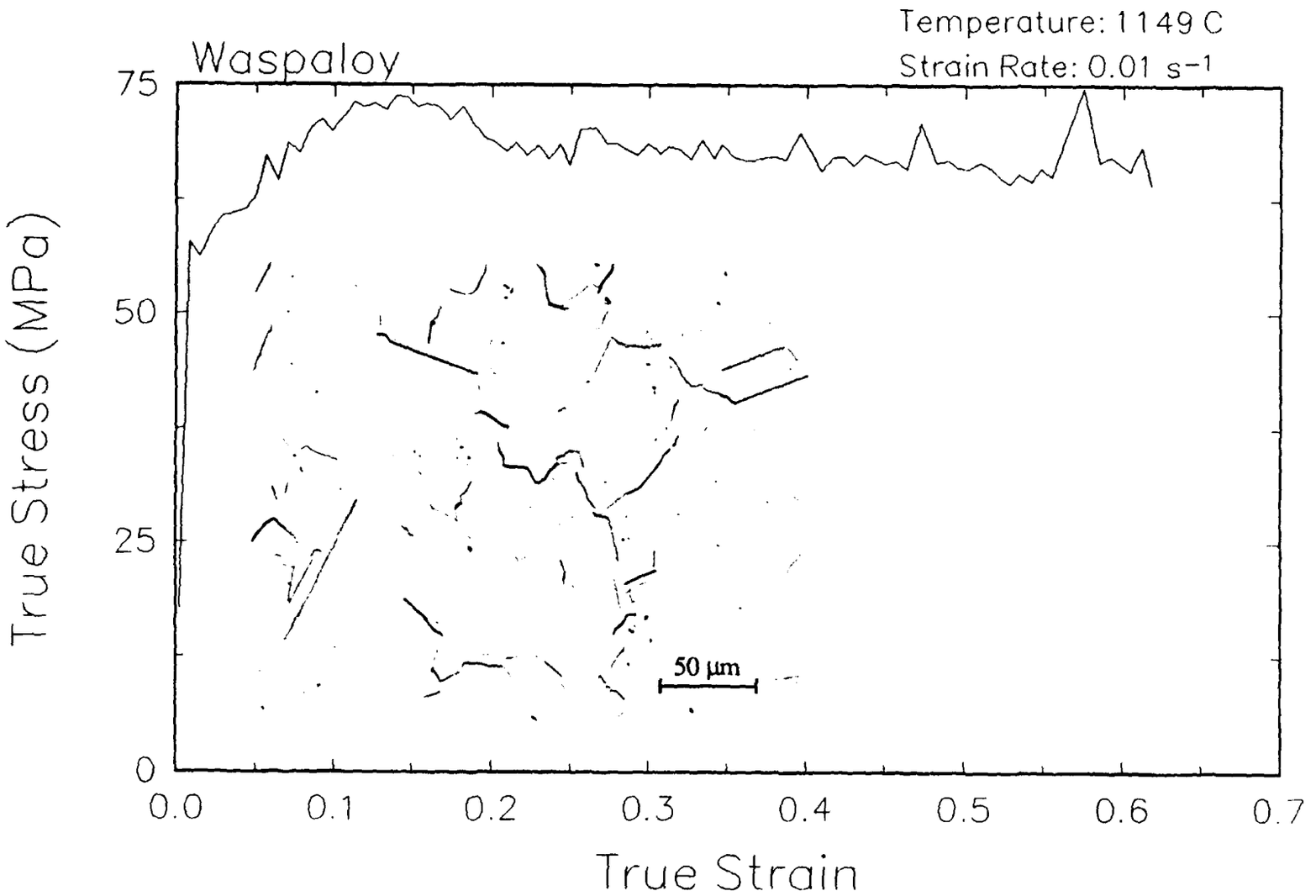

Figure 18. True stress-true strain curve and an optical micrograph from the center of the compressed sample cut through the compression axis, 1149 C and 0.01 s^{-1}.

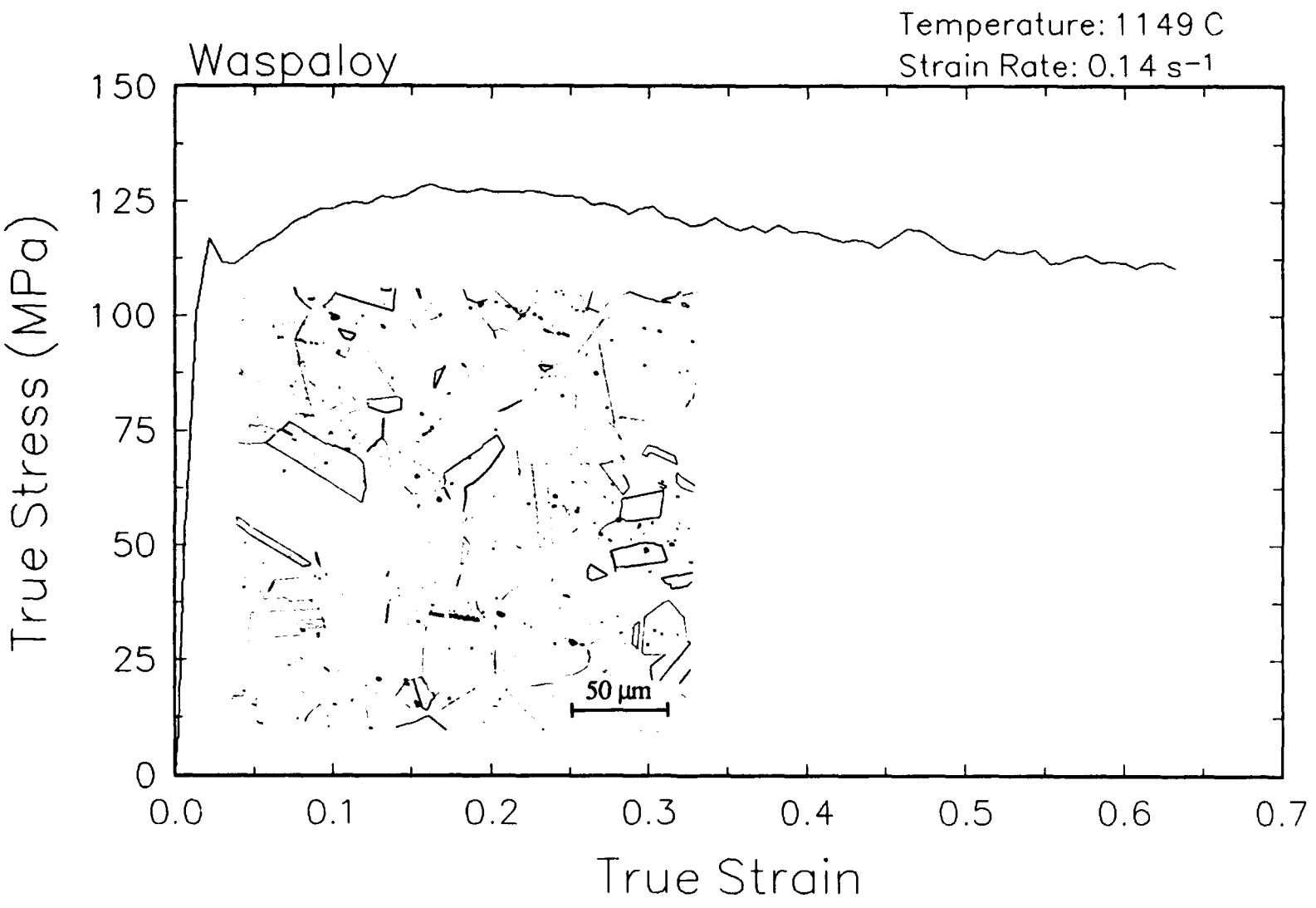

Figure 19. True stress-true strain curve and an optical micrograph from the center of the compressed sample cut through the compression axis, 1149 C and 0.14 s^{-1}.

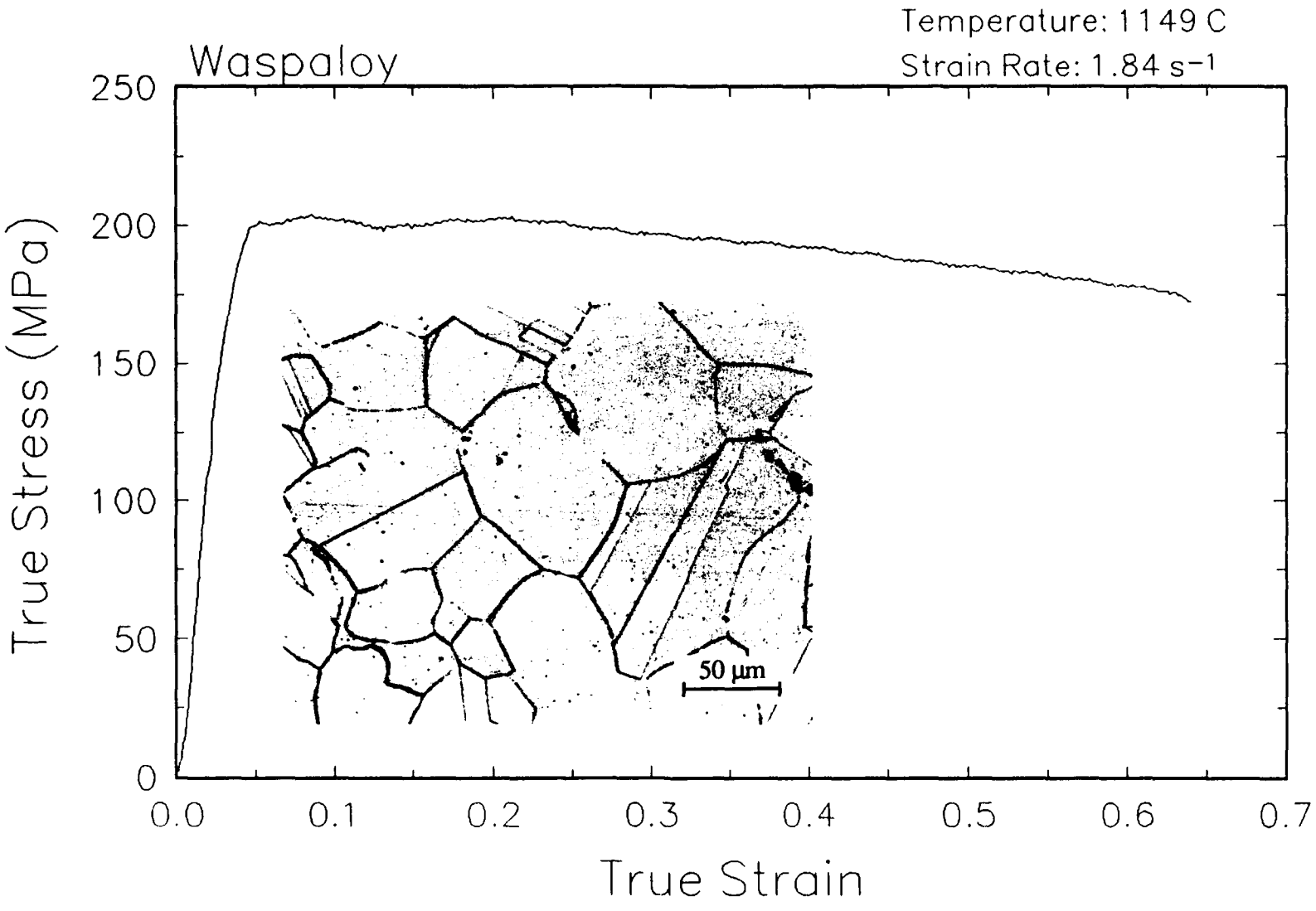

Figure 20. True stress-true strain curve and an optical micrograph from the center of the compressed sample cut through the compression axis, 1149 C and 1.84 s^{-1}.

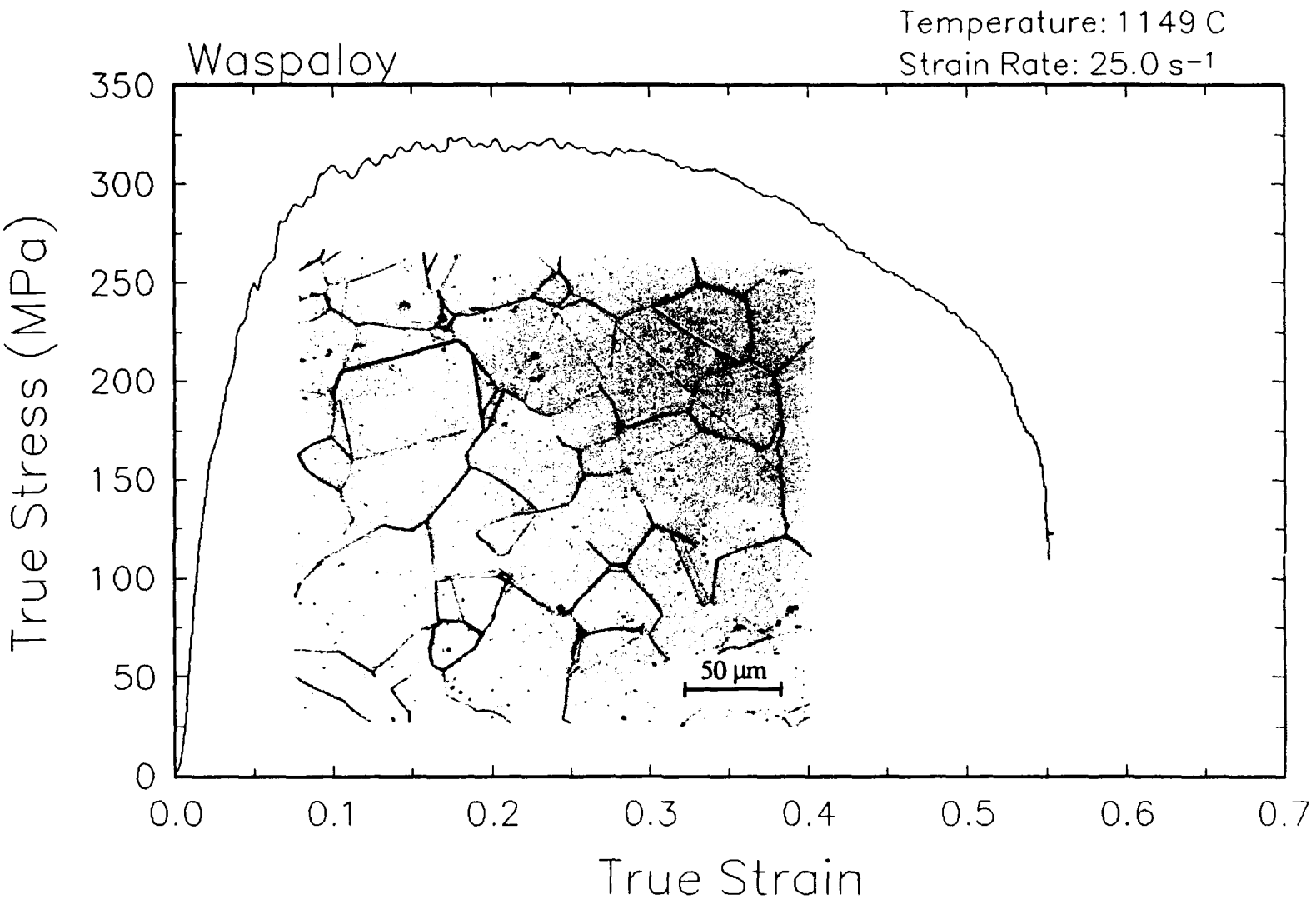

Figure 21. True stress-true strain curve and an optical micrograph from the center of the compressed sample cut through the compression axis, 1149 C and 25 s^{-1}.

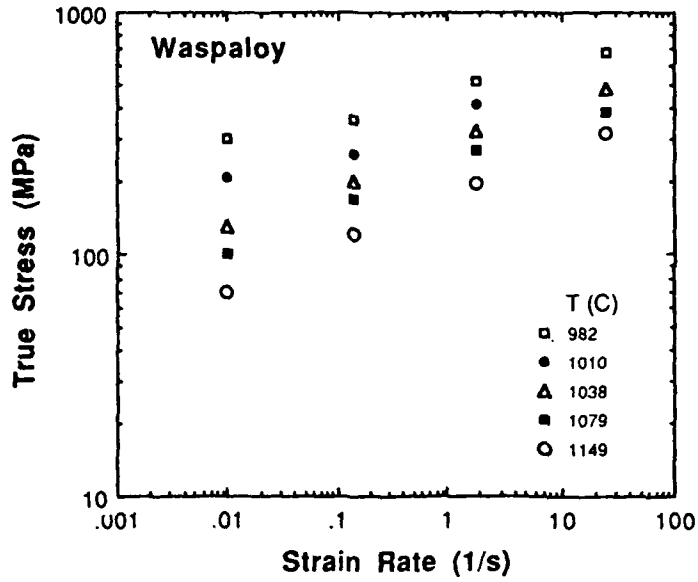

Figure 22. Effect of strain rate on stress in log-log scale at a true strain of 0.5 for Waspaloy.

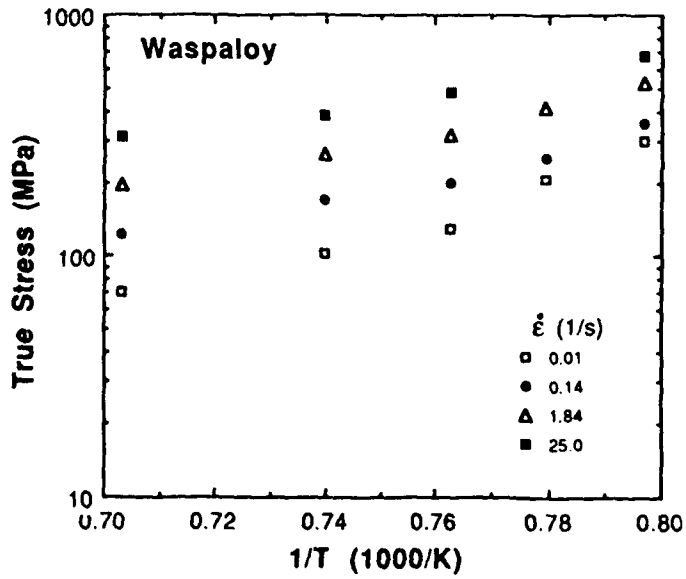

Figure 23. Effect of temperature on stress at a true strain of 0.5 for Waspaloy.

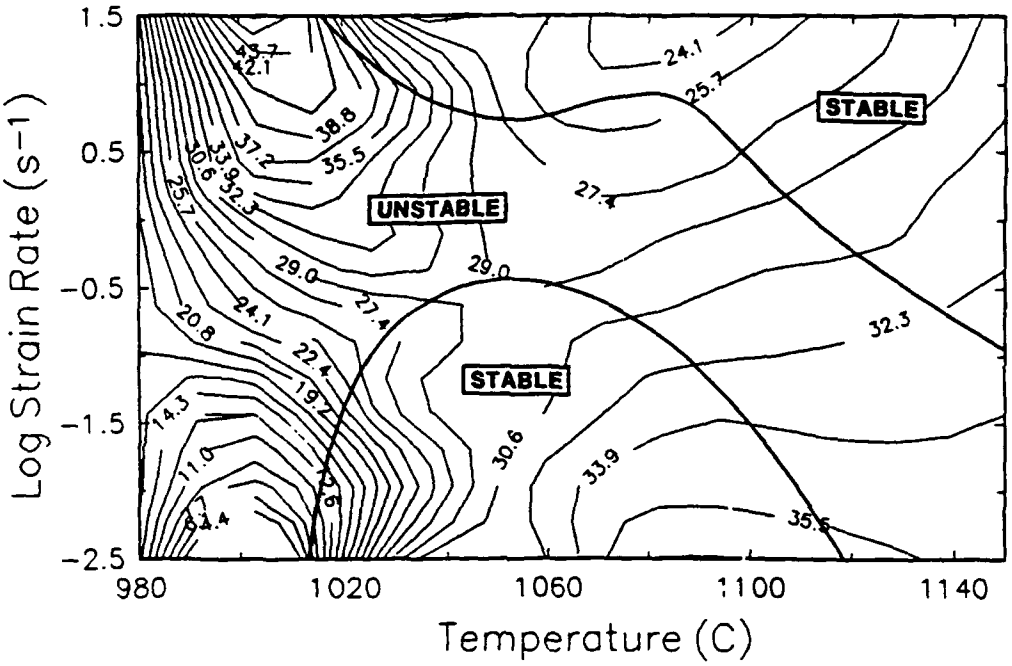

Figure 24. Processing map of Waspaloy at a true strain of 0.5.

Summary

Compression tests have been performed on Waspaloy over a range of temperatures and strain rates. The experimental conditions used in this work are representative of those used in metalforming practices. From the stress-strain curves, the flow behavior was characterized and a map which indicates the optimum processing condition was generated. This condition is approximately 1080 C and 0.01 s^{-1}.

The deformed microstructures were characterized from the as-quenched specimens by optical microscopy and are presented for each testing condition together with the stress-strain curves. Dynamic recovery. dynamic recrystallization and grain growth occurred over the temperature and strain rate range tested.

Implementation of Data Provided by the Atlas of Formability

The Atlas of Formability program provides ample data on flow behavior of various important engineering materials in the temperature and strain rate regime commonly used in metalworking processes. The data are valuable in design and problem solving of metalworking processes with advanced materials. Microstructural changes with temperature and strain rates are also provided in the Bulletin, which helps the design engineer to select processing parameters leading to the desired microstructure.

The data can also be used to construct processing map using dynamic material modeling approach to determine stable and unstable regions in terms of temperature and strain rate. The temperature and strain rate combination at the highest efficiency in the stable region provides the optimum processing condition. This has been demonstrated in this Bulletin. However, in some metalworking processes such as forging, strain rate varies within the workpiece. An analysis of the process with finite element method (FEM) can ensure that the strain rates at the processing temperature in the whole workpiece fall into the stable regions in the processing map. Furthermore, FEM analysis with the data from the Atlas of Formability can be coupled with fracture criteria to predict defect formation in metalworking processes.

Using the data provided by the Atlas of Formability, design of metalworking processes, dynamic material modeling, FEM analysis of metalworking processes, and defect prediction are common practice in Concurrent Technologies Corporation. Needs in solving problems related to metalworking processes can be directed to Dr. Prabir K. Chaudhury, Manager of the Atlas of Formability project, by calling (814) 269-2594.